Check for updates

ADVANCING EARTH AND SPACE SCIENCE

Geophysical Research Letters

RESEARCH LETTER
10.1029/2021GL093941

Key Points:

- Dynamic earthquake rupture simulations of the Cascadia Subduction Zone (CSZ) offshore Washington and Oregon region to investigate updip rupture behavior
- Larger tsunami amplitudes observed for the Oregon region suggest a large tsunami hazard in central and southern Cascadia
- Different orientations of the splays within the CSZ forearc result in differences in the amount of slip and tsunami heights

Supporting Information:

Supporting Information may be found in the online version of this article.

Correspondence to:

K. S. Aslam,
kaslam@uoregon.edu

Citation:

Aslam, K. S., Thomas, A. M., & Melgar, D. (2021). The effect of fore-arc deformation on shallow earthquake rupture behavior in the Cascadia subduction zone. *Geophysical Research Letters*, *48*, e2021GL093941. https://doi.org/10.1029/2021GL093941

Received 2 MAY 2021
Accepted 10 OCT 2021

Author Contributions:

Formal analysis: Khurram S. Aslam
Funding acquisition: Amanda M. Thomas
Investigation: Khurram S. Aslam
Project Administration: Amanda M. Thomas, Diego Melgar
Supervision: Amanda M. Thomas, Diego Melgar
Visualization: Khurram S. Aslam
Writing – original draft: Khurram S. Aslam
Writing – review & editing: Amanda M. Thomas, Diego Melgar

© 2021. American Geophysical Union. All Rights Reserved.

The Effect of Fore-Arc Deformation on Shallow Earthquake Rupture Behavior in the Cascadia Subduction Zone

Khurram S. Aslam[1], Amanda M. Thomas[1], and Diego Melgar[1]

[1]Department of Earth Sciences, University of Oregon, Eugene, OR, USA

Abstract Within the fore-arc of the Cascadia Subduction Zone, there are significant along-strike differences in the orientation of splay faults, sediment consolidation, and fault roughness. Here, we use dynamic rupture simulations of megathrust earthquakes on different realizations of a fault system that incorporate fore-arc properties representative of offshore Oregon and Washington to estimate how splay faults may behave in future megathrust earthquakes in Cascadia. While splay faults were activated in all of our simulations, splay orientation is a primary control on slip amplitude. Seaward vergent faults accommodate significant amounts of slip resulting in large seafloor uplift and significantly larger tsunami amplitudes. For example, our median tsunami heights including splay faults are about a factor of two larger than those that did not include splay fault deformation. We suggest that there is an urgent need to revisit existing approaches to tsunami hazard assessment in Cascadia to include the influence of splay faults.

Plain Language Summary The Cascadia subduction zone has hosted many great earthquakes in the past. Due to the potential of generating great earthquakes, this zone poses a huge earthquake and tsunami hazard. The main fault (or Cascadia megathrust) responsible for generating great earthquakes is about ~1,000-km long and is inferred to have variation in the geometrical and mechanical properties. One such difference is the difference between properties of the "forearc" region. The "forearc" is the shallow subsurface region on the landward side adjacent to the Cascadia megathrust. The orientation of the secondary faults (i.e., splays) is different in the forearc for the offshore Washington and Oregon region. Similarly, the consolidation of sediments within the forearc is also different for the Washington and Oregon region. In this study, we performed earthquake and tsunami simulation to understand how the difference in these forearc properties affects the tsunami hazard of the region. We found that the tsunami hazard in the Washington region is higher as compared to the Oregon region due to higher magnitude slip on the splay and megathrust. We find that this difference is mainly due to the difference in the orientation of splay faults.

1. Introduction

Many paleo-seismic studies find that the Cascadia subduction zone (CSZ) has the potential to produce great earthquakes (Goldfinger et al., 2012, 2017; Kelsey et al., 2002), and large tsunamis (Atwater et al., 2005; Satake et al., 2003). Based on historic tsunami records, the last great earthquake on the CSZ occurred in 1700 AD (Yamaguchi et al., 1997), was approximately a magnitude 9, and generated a trans-oceanic tsunami (Satake et al., 2003). Models of this earthquake suggest that there were along-strike differences in the slip distribution on the megathrust (Leonard et al., 2010; Wang et al., 2013), some of which correlate well with variations in megathrust geometry (e.g., subducting seamounts) (Wang et al., 2013).

Today, it is well recognized that there are significant along-strike geometrical and mechanical variations of the CSZ boundary thrust (Delph et al., 2021; Flueh et al., 1998; Goldfinger et al., 2017; Gulick et al., 1998; Han et al., 2017). For example, the CSZ fore-arc offshore Washington is mainly characterized by landward-vergent splay faults, while the fore-arc offshore central and southern Oregon is characterized by seaward-vergent splay faults (Adam et al., 2004; Booth-Rea et al., 2008; Cochrane et al., 1994; Gulick et al., 1998; MacKay, 1995). Consolidation of the accretionary wedge is different for the offshore Washington and offshore Oregon regions; Washington has sedimentary material with higher rigidity than Oregon

(Han et al., 2017). In addition, the downgoing plate is inferred to be rougher offshore Oregon since it is more deformed (Gulick et al., 1998; McCrory et al., 2012), and actively subducting seamounts (Tréhu et al., 2012). Such variations in fore-arc properties can influence updip rupture propagation characteristics, resulting seafloor displacements, and tsunami generation affecting the overall seismic and tsunami hazard of the region.

Previous dynamic rupture modeling studies focused on Cascadia have investigated downdip megathrust rupture behavior (Ramos & Huang, 2019) and overall rupture characteristics (Lotto et al., 2019) but little attention has been devoted to the updip rupture process. In this study, we perform a set of 2D dynamic earthquake rupture simulations of the CSZ offshore Washington and Oregon to obtain a better understanding of how variations in forearc properties and megathrust geometry affect shallow earthquake rupture behavior. Specifically, we test whether the vergence direction affects activation of the splay faults, and evaluate how off-fault plastic strain, in the presence of splay faults, affects surface deformation. In addition, we investigate whether there are changes in fault slip due to either variations in sedimentary consolidation of the fore-arc wedge or fault roughness. For each of these properties, we show how they influence rupture of the shallow megathrust, splay faults, and seafloor deformation. Finally, we perform tsunami simulations to explore how the variations in surface deformation of different models affect tsunami hazard in Washington and Oregon.

2. Methods

Our rupture models consist of a gently dipping plate boundary thrust with steeper splay faults whose orientations are based on the active source imaging of Han et al. (2017) (Figures 1a–1c). In both models, we simulate roughness by applying a geometric model with self-similar fractality to the megathrust (Candela et al., 2012). The RMS roughness height (given in Equation S3 in Supporting Information S1) of the Oregon model is chosen to be larger than that of the Washington model to simulate the rougher character of the southern Oregon megathrust (Gulick et al., 1998; McCrory et al., 2012). We primarily perform simulations of earthquake rupture propagation using elastic material properties for the off-fault material assuming a two-layer earth model (Figures 1b and 1c). To incorporate differences in the consolidation of forearc sedimentary sequence we choose different material properties for the shallow layer i.e., an overconsolidated shallow layer with higher rigidity for the Washington model ($V_p^{\text{shallow}} = 4.0$ km/s, $V_s^{\text{shallow}} = 2.2$ km/s, $\rho^{\text{shallow}} = 2.2$ g/cm^3) as compared to the Oregon model ($V_p^{\text{shallow}} = 3.5$ km/s, $V_s^{\text{shallow}} = 1.8$ km/s, $\rho^{\text{shallow}} = 2.0$ g/cm^3). We also perform a simulation of the Washington and Oregon models where the shallow subsurface off-fault material is allowed to yield anelastically. In both models, the deeper layer has higher rigidity ($V_p^{\text{deep}} = 6.5$ km/s, $V_s^{\text{deep}} = 3.8$ km/s, $\rho^{\text{deep}} = 2.8$ g/cm^3) than the shallow layer.

We set initial stresses for our rupture models based on the critical/elastic wedge theory (Dahlen et al., 1984). In this approach the stress state of the elastic wedge is characterized by the ratio of principal stresses σ_1 and σ_3 ("sigma ratio"), and the angle, Ψ that σ_1 makes relative to the basal fault. For our model, we assume a depth-dependent σ_3 (given as $\sigma_3 = -\rho g z(1 - \lambda)$, where z is the depth below the seafloor, g is the Earth's gravitational acceleration (=9.8 m/s^2), and λ is the ratio of pore pressure to the lithostatic overburden pressure). We choose a Ψ value of 13.5, which reflects nearly horizontal maximum principal stress (DeDontney & Hubbard, 2012). We choose a λ value of 0.8 (average λ used by Lotto et al., 2019 for the CSZ) and perform 30 simulations of rupture propagation with different realizations of the fault roughness profile where the sigma ratio of each simulation (either the Washington or Oregon profile) is chosen randomly from a uniform distribution ranging between 2.4 and 2.9. Our chosen model parameters are provided in the Supporting Information S1.

We define a model with a total depth of 40 km to perform our simulations where the top 20 km represents the locked portion of the CSZ megathrust (Li et al., 2018; Schmalzle et al., 2014). We assume a sigma ratio of 1 below 30 km depth to represent the low-effective stresses thought to operate in the region hosting episodic tremor and slip (e.g., Royer et al., 2015). In all of our simulations, we assume that the stresses on the fault do not increase between 10 and 20 km depth (as shown in Figure 1d). Additionally, the stresses are calculated based on a decreasing linear gradient for the megathrust between 20 and 30 km depth. We refer to this region as the gap (or transition) region. We use the linear slip weakening friction law (SWF) (Andrews, 1976; Ida, 1972) with static friction value of 0.6, dynamic friction value of 0.2, and slip-weakening distance of 1 m

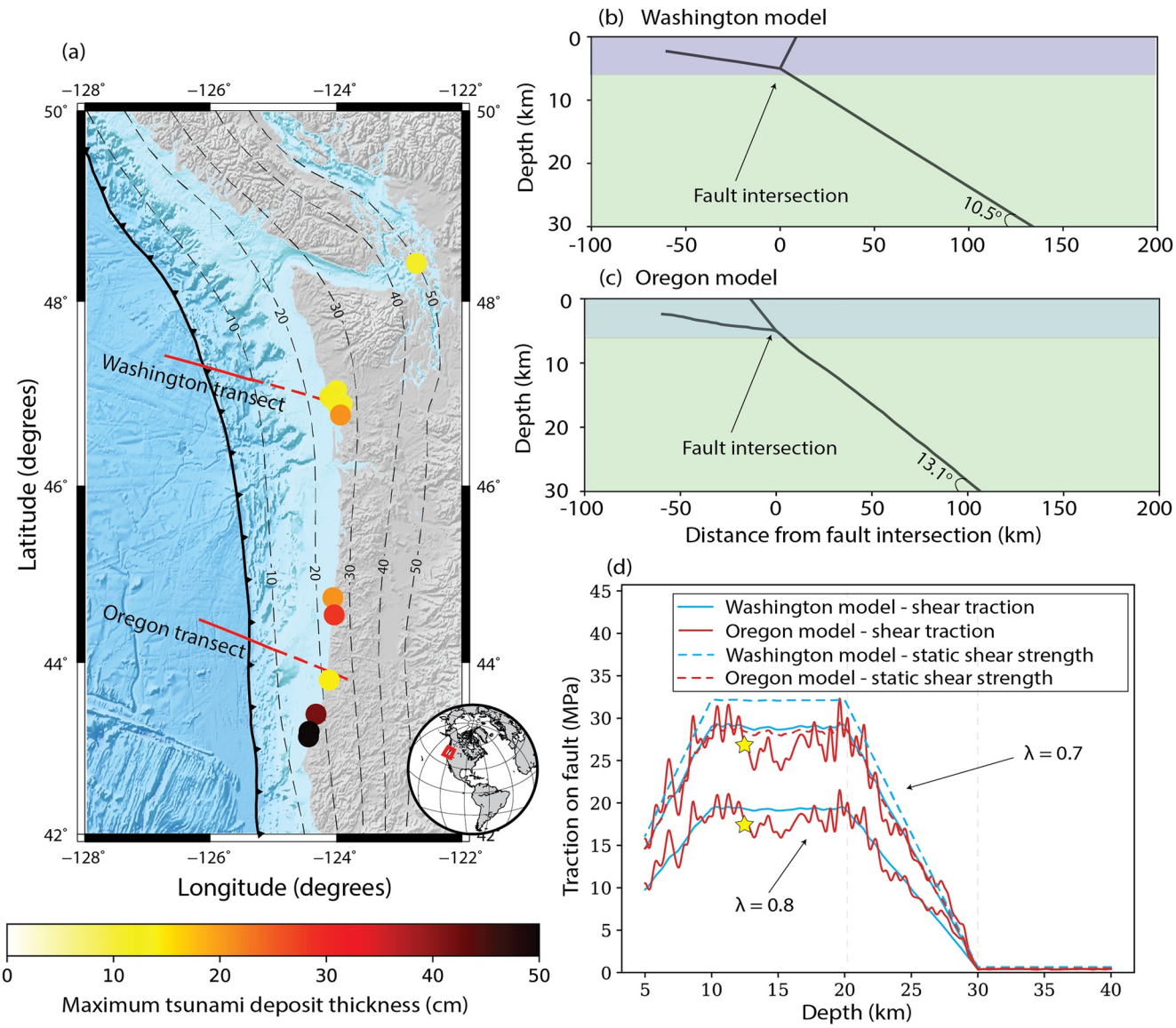

Figure 1. (a) Map of the CSZ. Black solid line (with triangles) shows the Cascadia deformation front. Red dashed lines show the Washington and Oregon transects of Han et al. (2017). Depth of the plate interface is indicated by dashed black lines (McCrory et al., 2012). The colored circles show the location of paleoseismic sites where tsunami deposit thicknesses are measured. (b) Model setup for the Washington profile. A two-segment megathrust fault is considered for dynamic earthquake rupture simulations. The splay fault is dipping landward (with steeper dip as compared to the main thrust). A two-layer earth model is considered, where the upper layer represents a consolidated (stiff) sedimentary layer. The boundary thrust fault has self-similar fractality with an RMS height of 0.001. (c) Model setup for Oregon profile. Same as (b), but with a rougher (RMS height = 0.01) and steeper megathrust. The sedimentary layer is softer for the Oregon profile and splay fault is seaward vergent. (d) Shear stress on the lower segment of the Washington and Oregon profile for $\lambda = 0.7$ and 0.8. Since the Oregon profile is rougher, we observe comparatively larger stress heterogeneities for the case of Oregon profile. The yellow star indicates the location of earthquake nucleation. Note that in each of the models, we only allow nucleation to occur at this location (details provided in S3 in Supporting Information S1).

to model friction on the basal fault. Details of all of our chosen values of the slip weakening parameters are provided in Table S1 in Supporting Information S1. Note that slip-strengthening friction is only applied to the portion of the splay fault that is within 2 km of the surface. We also run a model simulation assuming inelastic off-fault material properties for the shallow layer (top 6 km) of our model (described by Drucker–Prager viscoplasticity [Drucker & Prager, 1952], which is provided in S2 in Supporting Information S1). The closeness to failure ratio (CF ratio) describes how close the off-fault material is to failure (e.g., a material with a CF ratio of one is at the failure strength). We choose an initial CF ratio of 0.7 for the shallow layer which is implemented by choosing a variable cohesion value for each grid point, based on Equation 2. We

choose an earthquake nucleation depth of 13 km in all of our rupture models (details in S3 in Supporting Information S1). Finally, we simulate the tsunami that would result from our modeled rupture scenarios (details in S5 in Supporting Information S1) by solving the 1D non-linear shallow water equations using the final vertical seafloor displacement profiles as the initial condition (LeVeque et al., 2011).

3. Results and Discussion

Our simulations indicate that the rupture behavior on the deep portion of the megathrust is similar for both models. Figures 2a and 2b show the initial distribution of slip on the megathrust for different values of the sigma ratio. In both the Washington and Oregon models, larger sigma ratios have higher dynamic stress drops and hence higher resulting slip amplitudes. By comparing the deeper portion (>14 km) of the Washington and Oregon models at similar sigma ratios, we observe that the overall slip magnitudes of both the models is comparable. Because the megathrust is more steeply dipping in Oregon the rupture extends to greater depth in the same time period. Additionally, a noteworthy feature of both models is that a supershear transition occurs within the gap region (Figures 2c and 2d). This transition is a direct result of our parameterization of the shear stress and strength of the megathrust between the seismogenic zone and the region hosting ETS (Andrews, 2010) and is consistent with the results of Ramos and Huang (2019) and Ramos et al. (2021).

In contrast to the deeper fault, the simulated behavior of the shallow section of the megathrust is significantly different between the two models. We observe activation of splay faults in all of our simulations for both profiles. However, in comparing the splay fault slip between models (Figures 2e and 2f), we observe that the slip on the splay fault in the Oregon model is significantly larger than that in the Washington model. For example, the splay fault slip for the lowest sigma ratio simulations are shown in Figures 2e and 2f. These simulations predict an average slip of ∼25 m for the Washington model, and ∼50 m for the Oregon model. This difference can be attributed to variations in both geometry and material properties. The splay faults in the Oregon model are buried in sediments with lower rigidity (as compared to the splay faults in the Washington model), which promotes larger slip on these faults. Additionally, these seaward vergent faults are more favorable for rupture propagation as no slip is observed for the upper megathrust segments in these models as can be seen in Figures 2e and 2f.

In addition, Figures 2e and 2f, show that the slip amplitude of the Oregon fault profile is more heterogeneous than the Washington profile. This is more obvious for the case of Oregon model with sigma ratio of 2.62 (or comparing Figures S3f and S4f in Supporting Information S1). This behavior is a direct consequence of the larger fault roughness in the Oregon simulations (Bruhat et al., 2016; Dunham et al., 2011; Fang & Dunham, 2013) and results in only local changes in fault slip (due to local stress heterogeneities on the fault as shown in Figure 1d). It does not affect the overall slip magnitude in our simulations. Note that a similar result has been observed in the dynamic rupture simulations on rough faults by Dunham et al. (2011), however analysis of Dieterich and Smith (2009) assuming quasi-static slip on the rough fault show an overall increase in the fault slip with decrease in RMS roughness height of the fault. Fault roughness also affects the rupture propagation (as the rupture changes its speed during its propagation through local geometrical heterogeneities), resulting in the generation of high frequency seismic radiation (Dunham et al., 2011), which are observed in synthetic seismograms calculated for the Oregon models (Figure S5a in Supporting Information S1).

Several features of our simulation results have direct implications for ground motions in a future CSZ earthquake. First, supershear ruptures result in amplified ground motions at farther distances as compared to typical sub-shear ruptures (Andrews, 2010). As such, our modeling results suggest that for both Washington and Oregon stronger ground motions may be expected further onshore for a large CSZ earthquake than those determined from regional ground motion prediction equations. Second, the peak ground velocity (PGV) is larger for the Oregon models at near-fault distances (Figure S5 in Supporting Information S1) owing to larger slip of the basal megathrust and splay faults at shallower depths. The near-fault ground motions also have longer duration for the Oregon models as compared to the Washington model. The PGV values for the Oregon models at far fault distances are comparable to the Washington model due to the steeper geometry of the Washington models and proximity of the station to the splay fault in the Washington model.

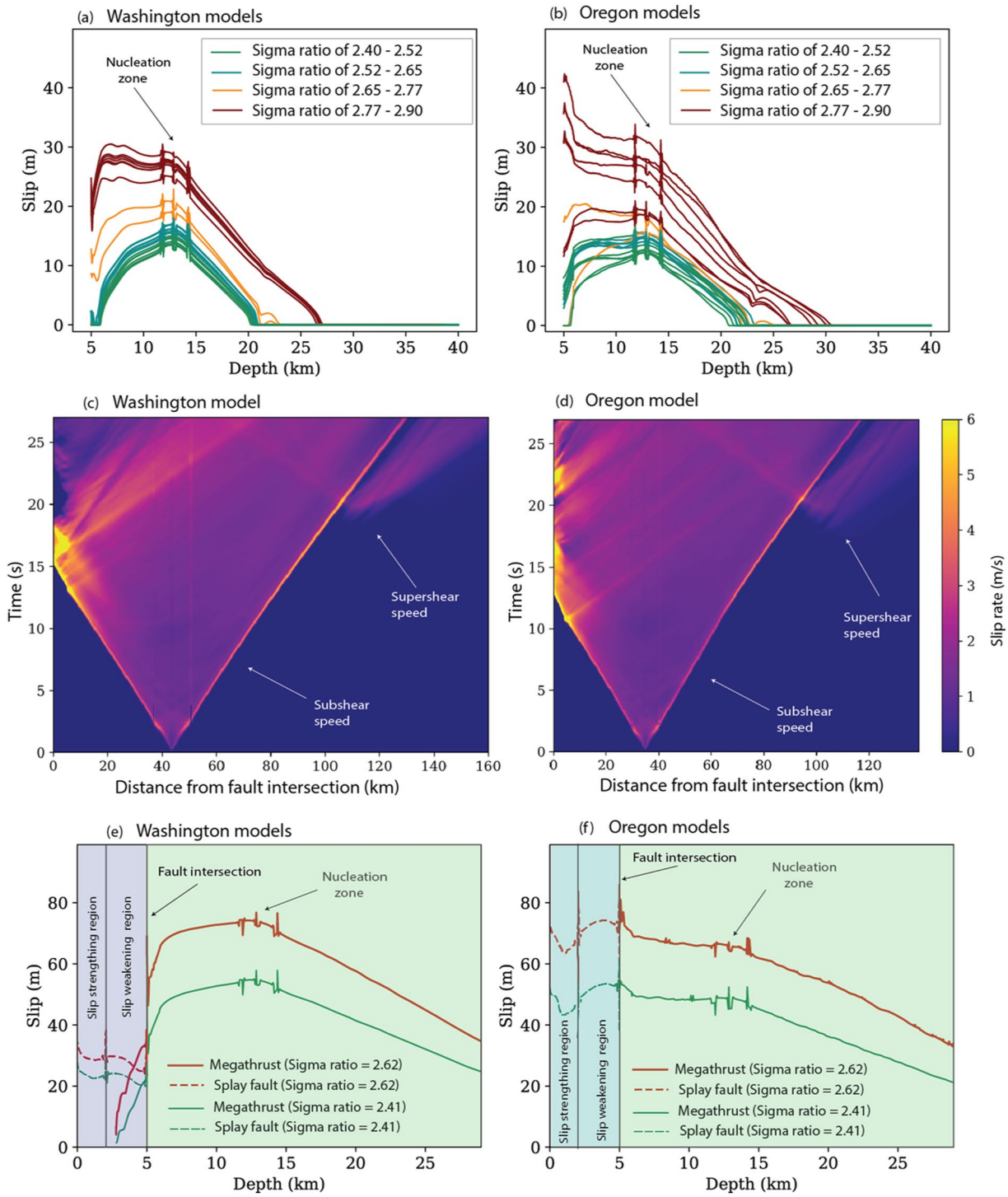

Figure 2. (a) Slip on the megathrust in the Washington models for different sigma ratios i.e., the ratio of principal stresses $\sigma 1$ and $\sigma 3$ (between 2.4 and 2.9) at time $t = 13.5$ s. (b) Same as (a), but for the Oregon profile. Different stress ratios lead to different magnitudes of slip, but overall behavior remains the same. Rupture on the Oregon profile reaches to deeper depths at similar times since the Oregon fault has a steeper geometry than the Washington model. The slip is larger at shallower depths for the Oregon fault profiles. (c) Slip rate history (in time-space) of the rupture on the Washington megathrust with sigma ratio of 2.62. The distance shown along the *x*-axis is the distance along the fault. (d) Same as (c), but for the Oregon megathrust. (e) Slip on the megathrust and the splay fault of two Washington models at time $t = 42.7$ s. The slip on the splay fault is less than the slip on the main boundary thrust. (f) Same as (e), but for the Oregon models. The slip on the splay fault is comparable to the slip on the main boundary thrust.

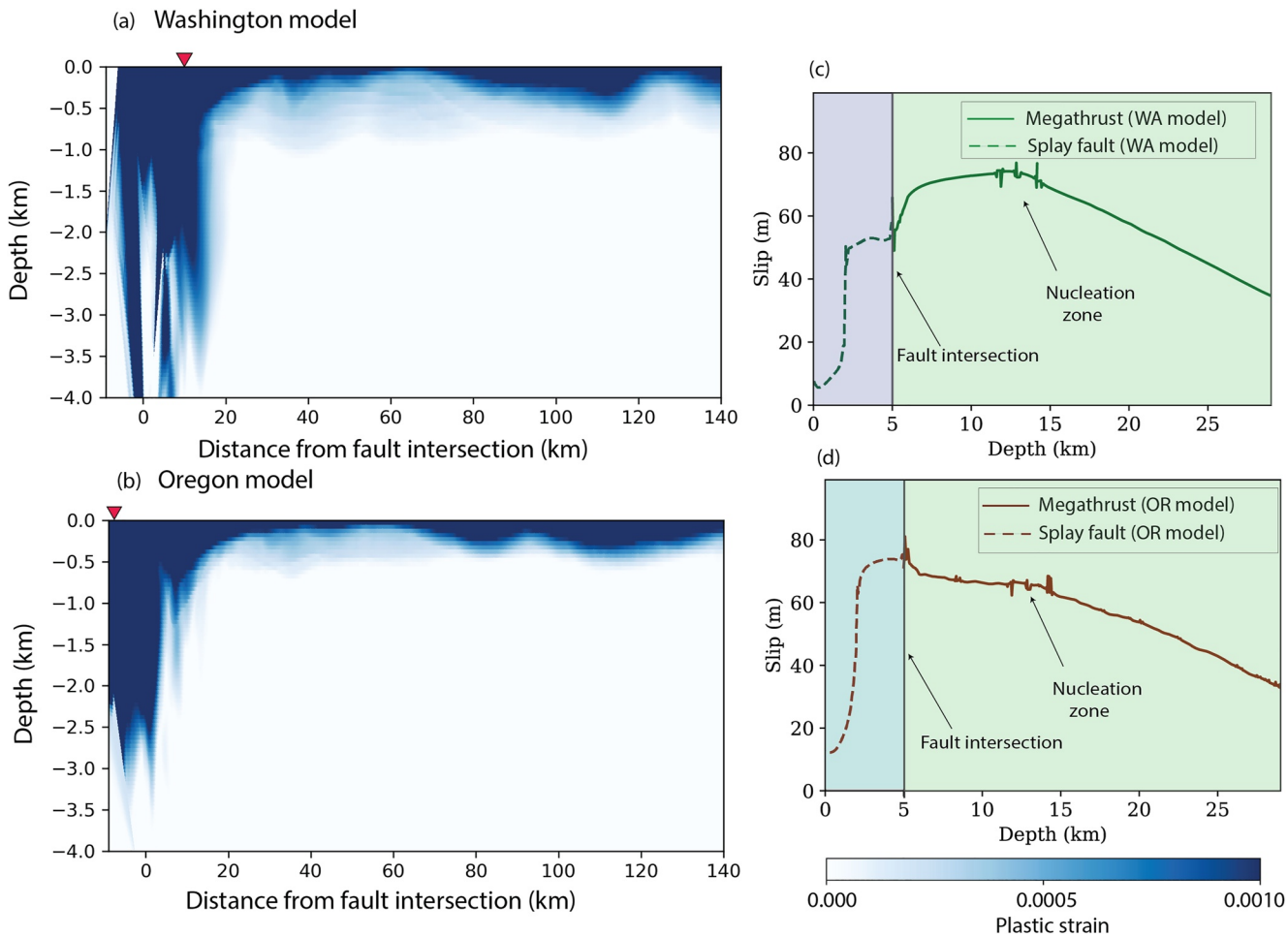

Figure 3. (a) Plastic strain accumulation for the Oregon model (shown in Figure 1) at time $t = 42.7$ s when initial sigma ratio is 2.62. (b) Same as (a), but for the Washington model (shown in Figure 1). Note that the inverted triangle in both (a) and (b) marks the upper edge of the splay faults while the bottom edge of the fault is at the fault intersection (0 value of the *x*-axis). (c) Slip on the splay fault and the basal thrust of the Washington model. (d) Same as (c), but for the Oregon model. A distinction of slip behavior of the splay fault is observed between the slip-weakening and slip-strengthening region for both models while the slip on the splay fault of the Washington model is lower than the splay of the Oregon model.

Finally, larger fault roughness in the Oregon model increases the amount of high frequency seismic radiation (Figure S6 in Supporting Information S1).

To determine how anelastic off fault material properties may affect the above results we perform two additional simulations that incorporate such properties. Figures 3a and 3b shows the plastic strain accumulation for the Washington and Oregon models (the same fault profiles shown in Figure 1). The overall behavior of plastic strain accumulation remains similar for the two models. This occurs because the yielding of the material is sensitive to the CF ratio, and we assume the same CF ratio for both the Washington and Oregon models. Regions which are closer to the splay fault show significant plastic strain accumulation as compared to the regions that are farther from the splay fault. Anelastic deformation adjacent to the faults is higher since that region is characterized by strong changes in static and dynamic stress (Ma, 2012). The shallower part (<1 km depth) of our model domain (away from the splay fault) shows higher anelastic deformation as compared to the deeper fault which can be important for resulting uplift and tsunami excitation. This happens due to the low confining pressure at shallower depths resulting in a widespread yielding of the shallower low-cohesion material (Ma & Nie, 2019). Our plastic simulations (Figures 3c and 3d) show that the overall behavior of the slip profile on the deeper part of the megathrust splay of the Washington and Oregon model remains similar to what is observed for the rupture models with elastic off-fault material properties. Similar to the elastic models, the activation of the splay faults occurs in both the Oregon and the

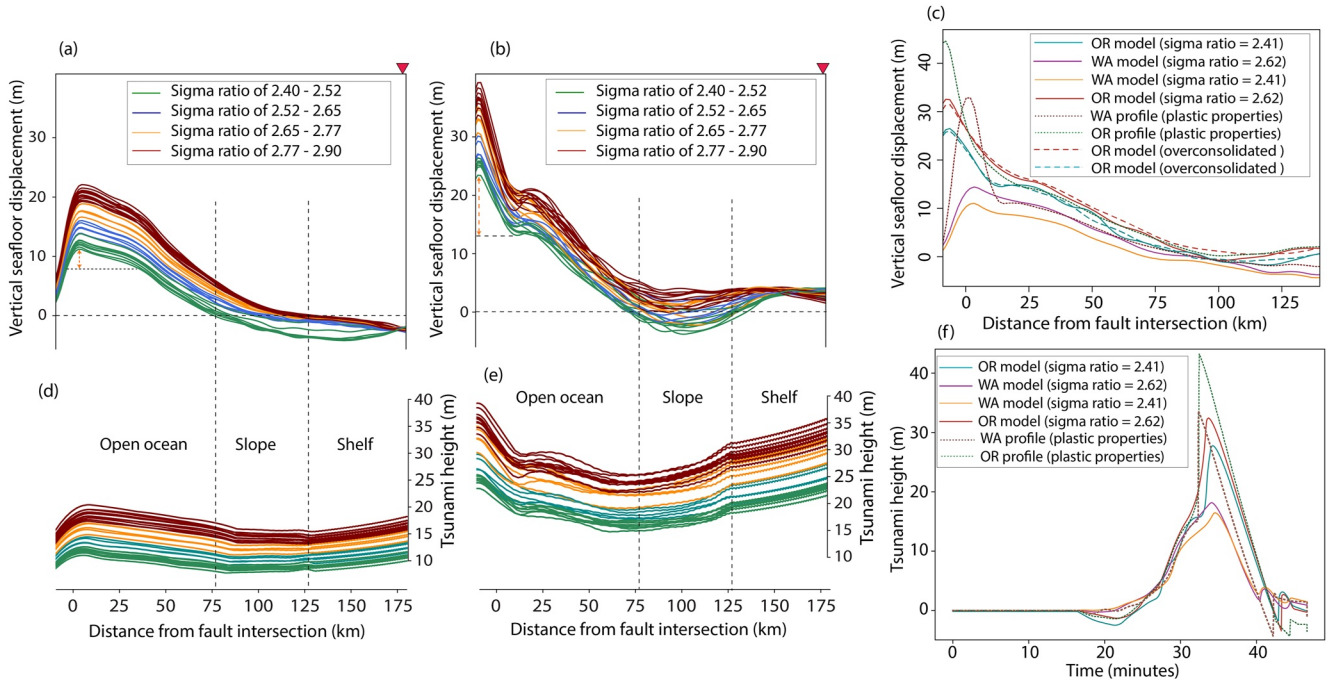

Figure 4. (a) Vertical seafloor displacements (uplift) of Washington models for different values of sigma ratios (between 2.4 and 2.9) at time $t = 100.2$ s. (b) Same as (a), but for the Oregon models. The Oregon models have higher values of seafloor uplift as compared to the Washington models (above the splay fault). (c) Vertical seafloor displacement (uplift) for the models shown in Figures 2c, 2d, 3c and 3d. The dashed lines are uplift for the Oregon model but with sediment consolidation similar to the Washington models (slip of the consolidated model is provided in Figure S9 in Supporting Information S1). Comparison of dashed and solid line of the Oregon models suggests that the sediment consolidation does not play a significant role in increasing the seafloor uplift above the splay faults. Uplift for the model with anelastic off-fault properties show higher uplift as compared to the model with elastic off-fault properties. (d) Maximum tsunami heights as a result of tsunami simulations based on the vertical uplift shown in (a). (e) Maximum tsunami heights as a result of tsunami simulations based on the vertical uplift shown in (b). The open ocean in (d) and (e) represents the region with bathymetric depth of 4,500 m. The slope region is where depth decreases from 4,500 to 50 m and the shelf is region having depth of 0–50 m. (f) Wave height recorded at the gauge location (red inverted triangle) for the 48 min of the tsunami simulation. The maximum wave height of the Oregon models is significantly higher than the maximum wave height of the Washington models.

Washington model while the overall slip on the splay fault (and shallower part of megathrust) is larger for the Oregon model. Note that the slip amplitudes in the slip-strengthening region (<2 km depth) are significantly lower for the anelastic models as compared to the elastic models.

We observe activation of the splay faults in all of our models, irrespective of the chosen orientation, which manifests as larger vertical seafloor deformation (Figure 4) at locations where the splay faults intersect the seafloor (−10 and 10 km from fault intersection). The overall behavior of the uplift remains similar for different sigma ratios for the Oregon and Washington model that is, we observe higher uplift values for larger sigma ratios. Note that the Oregon model (i.e., Figure 4b) shows significantly larger uplift above the splay fault (shown by dashed orange line) as compared to the Washington models (i.e., Figure 4a); this (Figures 4a and 4b) is due to the difference in the slip magnitude of the splay fault which results from differences in sediment consolidation of the shallow fore-arc material and splay fault orientation. To explore the contribution of sediment consolidation of the Oregon model to the uplift, we run an additional simulation of two Oregon models (shown in Figure 2f) while keeping their sediment consolidation similar to the Washington models. We refer to these models as overconsolidated Oregon models. Our comparison of uplift between overconsolidated and underconsolidated Oregon models (Figure 4c, comparing dashed and solid lines) suggests that differences in sediment consolidation do not significantly change the seafloor uplift above splay faults of Oregon model. This is because there are not large differences in elastic properties between the two models: this result highlights the dominant role of splay orientation in controlling uplift. Note that a significantly large difference in rigidity between two models may result in more pronounced difference in slip amplitude (Lotto et al., 2017). The model with anelastic deformation of the shallow subsurface material shows even larger vertical seafloor displacements above the splay faults (Figure 4c) since for this model the uplift

observed are the sum of uplift due to slip on the splay fault and the uplift due to an-elastic deformation of the material (Ma, 2012; Ma & Nie, 2019; Wilson & Ma, 2021).

Our tsunami simulation results (Figures 4d and 4e) show a similar trend to what is observed for the vertical seafloor deformation. We observe larger tsunami amplitudes for the models with larger uplift (i.e., higher sigma ratios) and hence a larger predicted tsunami for the Oregon model. There are small variations in the tsunami height (Figures 4d and 4e), which are merely due to our assumed initial bathymetry of the seafloor (details in S5 in Supporting Information S1). One such effect is the amplification and shortening of wavelength of the tsunami wave (Figure S10 in Supporting Information S1) due to shoaling once it reaches the shelf (George et al., 2020). Based on the wave height recorded at a gauge station (Figure 4f) placed at the location shown by the inverted triangle in Figure 4, we observe that the maximum wave height is recorded at a slightly earlier time for the Washington models as compared to the Oregon models. This happens because the location of maximum vertical uplift is closer to the shoreline for the Washington model (as the splay fault is landward vergent). Although the maximum wave height is recorded at a slightly later time for the Oregon profile, the maximum wave height recorded for the Oregon profile is still significantly larger than that of the Washington model. Although our tsunami simulations do not incorporate the effect of concave geometry of the coastline of the CSZ, this geometry may further enhance the tsunami amplitudes in central Oregon. In addition, our 2D model with splay faults may overestimate the tsunami hazard of a M9 CSZ event (due to limited extent of splay faults in nature) but these results are of significant importance for the local tsunami hazard of Oregon and Washington region since a local increase in the vertical seafloor uplift results in a local increase in tsunami amplitudes at the closest shoreline region (Melgar et al., 2019; Salaree et al., 2021).

Several paleoseismic studies (e.g., Peterson & Darienzo, 1996; Schlichting, 2000; Shennan et al., 1996) have reported the thickness of tsunami deposits related to large earthquakes that occurred on the Cascadia megathrust in the past. Shennan et al. (1996) observed a maximum tsunami deposit thickness of 2 and 4 cm in southern Washington. Moving further south (within southern Washington) from sites of Shennan et al. (1996), the maximum tsunami deposit thickness increased to 5 cm (Schlichting, 2000). For most of the sites of southern Washington, the maximum tsunami deposit remained below 10 cm (Atwater, 1987). Only one study (Atwater & Hemphill-Haley, 1997) has reported a maximum tsunami deposits thickness of 15 cm in southern Washington. In the Oregon region, although some sites have reported a maximum tsunami deposit thickness of 10 cm (Peterson & Priest, 1995), 15 cm (Darienzo et al., 1994), and 25 cm (Peterson & Darienzo, 1996), there are sites (in the central and southern Oregon region) where maximum tsunami deposit thickness was reported as high as 50 and 150 cm (Kelsey et al., 1998). The higher tsunami deposit thickness observed in the central Oregon may indicate a larger amplitude tsunami occurred in this region (as suggested by our results), but this conclusion is not definitive since the tsunami deposit thickness can also be influenced by other factors such as flow velocity, water depth, topography, and sediment supply.

Tsunami hazard assessments of the CSZ region are driven strongly by earthquake and tsunami models (Witter et al., 2013) since there is only one instance of a modern-day tsunamigenic event (González et al., 1995). These models are, at present, based on oversimplified assumptions. For example, they assume at worst non-realistic homogeneous slip distribution across the whole megathrust (Priest et al., 1997, 2000) and at best (e.g., Priest et al., 2009; Witter et al., 2013) simplified slip heterogeneity, by dividing the whole megathrust into four segments and then assuming similar slip distribution within each of these segments. Using this approach, the most hazardous M9 scenario assumed by Witter et al. (2013) produced a maximum wave height (of 14.8 m which is somewhat comparable to maximum wave height of 13.4 m from our overconsolidated model with no splay faults) at the shoreline which is still lower (by a factor of 2) than the median wave height suggested by our results and much lower than the amplitudes seen in recent large tsunamigenic events worldwide (Mori et al., 2011). None of the models currently used for hazards assessments include contributions from splay faulting, dynamic deformation, inelastic material response, or material heterogeneity, which we have shown plays an additional role in the overall hazard. The existing earthquake rupture models do not truly capture the complexity of behaviors possible at the CSZ. Somewhat alarmingly, the present simplifications might lead to an overall underestimation of the hazard. We suggest that there is a need to revisit the existing approaches to include some of the complexities we have discussed.

4. Conclusions

To conclude, we perform a set of 2D dynamic earthquake rupture simulations of the CSZ offshore Washington and Oregon incorporating differences in the consolidation of forearc sedimentary sequence, and the orientation of splay faults. Our results suggest that the likelihood of splay faults activating during great earthquakes on the CSZ megathrust does not strongly depend on their orientation. This finding is of particular importance for fault systems such as the CSZ where the megathrust does not intersect the seafloor, and hence slip on splay faults can significantly change the tsunami hazard of the region. We find that different orientations of the splays known to exist within the CSZ forearc result in differences in the amount of slip, seafloor uplift amplitude, resultant tsunami heights, and tsunami arrival times. We observe larger seafloor uplift and tsunami amplitudes for the Oregon region (where the splay faults are seaward vergent) as compared to the Washington region suggesting a large tsunami hazard in central and southern Cascadia. Our results suggest that the major contribution to the difference in uplift and tsunami amplitude comes from the variation in the angle of the splay fault, while other differences in parameters between the two primary model setups (such as material properties in the shallow layer and the angle of decollement) are of lesser importance. Finally, we have shown that the anelastic yielding of the sediments of the accretionary wedge of the CSZ can enhance the vertical seafloor deformation above the splays (as compared to elastic models) for both Oregon and Washington regions, which results in a larger tsunami as compared to the models without anelastic yielding.

Data Availability Statement

The code is freely available and can be downloaded from http://www.clawpack.org/geoclaw. This code and all the simulation data is available at https://zenodo.org/record/5228280 (https://doi.org/10.5281/zenodo.5228280).

Acknowledgments
This research work was supported by National Science foundation (NSF award no. 1663834). The authors thank Randall LeVeque for providing his help with the tsunami simulation code. The authors also thank Eric Daub for providing his earthquake dynamic rupture code.

References

Adam, J., Klaeschen, D., Kukowski, N., & Flueh, E. (2004). Upward delamination of Cascadia Basin sediment infill with landward frontal accretion thrusting caused by rapid glacial age material flux. *Tectonics*, *23*(3), TC3009. https://doi.org/10.1029/2002tc001475

Andrews, D. J. (1976). Rupture velocity of plane strain shear cracks. *Journal of Geophysical Research*, *81*(32), 5679–5687. https://doi.org/10.1029/jb081i032p05679

Andrews, D. J. (2010). Ground motion hazard from supershear rupture. *Tectonophysics*, *493*(3–4), 216–221. https://doi.org/10.1016/j.tecto.2010.02.003

Atwater, B. F. (1987). Evidence for great Holocene earthquakes along the outer coast of Washington State. *Science*, *236*(4804), 942–944. https://doi.org/10.1126/science.236.4804.942

Atwater, B. F., & Hemphill-Haley, E. (1997). *Recurrence intervals for great earthquakes of the past 3,500 years at northeastern Willapa Bay*. Washington: US Government Printing Office.

Atwater, B. F., Satoko, M. R., Kenji, S., Kazue, U., Yoshinobu, T., & Yamaguchi, D. K. (2005). *The orphan tsunami of 1700: Japanese clues to a parent earthquake in North America (No. 1707)*. US Geological Survey.

Booth-Rea, G., Klaeschen, D., Grevemeyer, I., & Reston, T. (2008). Heterogeneous deformation in the Cascadia convergent margin and its relation to thermal gradient (Washington, NW USA). *Tectonics*, *27*(4). https://doi.org/10.1029/2007tc002209

Bruhat, L., Fang, Z., & Dunham, E. M. (2016). Rupture complexity and the supershear transition on rough faults. *Journal of Geophysical Research: Solid Earth*, *121*(1), 210–224. https://doi.org/10.1002/2015jb012512

Candela, T., Renard, F., Klinger, Y., Mair, K., Schmittbuhl, J., & Brodsky, E. E. (2012). Roughness of fault surfaces over nine decades of length scales. *Journal of Geophysical Research*, *117*(B8), B08409. https://doi.org/10.1029/2011jb009041

Cochrane, G. R., Moore, J. C., MacKay, M. E., & Moore, G. F. (1994). Velocity and inferred porosity model of the Oregon accretionary prism from multichannel seismic reflection data: Implications on sediment dewatering and overpressure. *Journal of Geophysical Research*, *99*(B4), 7033–7043. https://doi.org/10.1029/93jb03206

Dahlen, F. A., Suppe, J., & Davis, D. (1984). Mechanics of fold-and-thrust belts and accretionary wedges: Cohesive Coulomb theory. *Journal of Geophysical Research*, *89*(B12), 10087–10101. https://doi.org/10.1029/jb089ib12p10087

Darienzo, M. E., Peterson, C. D., & Clough, C. (1994). Stratigraphic evidence for great subduction-zone earthquakes at four estuaries in northern Oregon, USA. *Journal of Coastal Research*, *10*, 850–876.

DeDontney, N., & Hubbard, J. (2012). Applying wedge theory to dynamic rupture modeling of fault junctions. *Bulletin of the Seismological Society of America*, *102*(4), 1693–1711. https://doi.org/10.1785/0120110190

Delph, J. R., Thomas, A. M., & Levander, A. (2021). Subcretionary tectonics: Linking variability in the expression of subduction along the Cascadia forearc. *Earth and Planetary Science Letters*, *556*, 116724. https://doi.org/10.1016/j.epsl.2020.116724

Dieterich, J. H., & Smith, D. E. (2009). Nonplanar faults: Mechanics of slip and off-fault damage. In *Mechanics, structure and evolution of fault zones* (pp. 1799–1815). Birkhäuser Basel.

Drucker, D. C., & Prager, W. (1952). Soil mechanics and plastic analysis or limit design. *Quarterly of Applied Mathematics*, *10*(2), 157–165. https://doi.org/10.1090/qam/48291

Dunham, E. M., Belanger, D., Cong, L., & Kozdon, J. E. (2011). Earthquake ruptures with strongly rate-weakening friction and off-fault plasticity, Part 2: Nonplanar faults. *Bulletin of the Seismological Society of America*, *101*(5), 2308–2322. https://doi.org/10.1785/0120100076

Fang, Z., & Dunham, E. M. (2013). Additional shear resistance from fault roughness and stress levels on geometrically complex faults. *Journal of Geophysical Research: Solid Earth*, *118*(7), 3642–3654. https://doi.org/10.1002/jgrb.50262

Flueh, E. R., Fisher, M. A., Bialas, J., Childs, J. R., Klaeschen, D., Kukowski, N., & Vidal, N. (1998). New seismic images of the Cascadia subduction zone from cruise SO108—ORWELL. *Tectonophysics*, *293*(1–2), 69–84. https://doi.org/10.1016/s0040-1951(98)00091-2

George, J., Ketcheson, D. I., & LeVeque, R. J. (2020). Shoaling on steep continental slopes: Relating transmission and reflection coefficients to Green's law. *Pure and Applied Geophysics*, *177*(3), 1659–1674. https://doi.org/10.1007/s00024-019-02316-y

Goldfinger, C., Galer, S., Beeson, J., Hamilton, T., Black, B., Romsos, C., et al. (2017). The importance of site selection, sediment supply, and hydrodynamics: A case study of submarine paleoseismology on the northern Cascadia margin, Washington USA. *Marine Geology*, *384*, 4–46. https://doi.org/10.1016/j.margeo.2016.06.008

Goldfinger, C., Nelson, C. H., Morey, A. E., Johnson, J. E., Patton, J. R., Karabanov, E. B., & Enkin, R. J. (2012). *Turbidite event history—Methods and implications for Holocene paleoseismicity of the Cascadia subduction zone (No. 1661-F)*. US Geological Survey.

González, F. I., Satake, K., Boss, E. F., & Mofjeld, H. O. (1995). Edge wave and non-trapped modes of the 25 April 1992 Cape Mendocino tsunami. In *Tsunamis: 1992–1994* (pp. 409–426). https://doi.org/10.1007/978-3-0348-7279-9_3

Gulick, S. P., Meltzer, A. M., & Clarke, S. H., Jr (1998). Seismic structure of the southern Cascadia subduction zone and accretionary prism north of the Mendocino triple junction. *Journal of Geophysical Research*, *103*(B11), 27207–27222. https://doi.org/10.1029/98jb02526

Han, S., Bangs, N. L., Carbotte, S. M., Saffer, D. M., & Gibson, J. C. (2017). Links between sediment consolidation and Cascadia megathrust slip behaviour. *Nature Geoscience*, *10*(12), 954–959. https://doi.org/10.1038/s41561-017-0007-2

Ida, Y. (1972). Cohesive force across the tip of a longitudinal-shear crack and Griffith's specific surface energy. *Journal of Geophysical Research*, *77*(20), 3796–3805. https://doi.org/10.1029/jb077i020p03796

Kelsey, H. M., Nelson, A. R., Hemphill-Haley, E., & Witter, R. C. (1998). Short-term and long term changes in ocean level recorded by a coastal freshwater meromitic lake, Cascadia subduction zone, southern Oregon. In *Geological society of America abstracts with programs* (Vol. 30, p. 162).

Kelsey, H. M., Witter, R. C., & Hemphill-Haley, E. (2002). Plate-boundary earthquakes and tsunamis of the past 5500 yr, Sixes River estuary, southern Oregon. *The Geological Society of America Bulletin*, *114*(3), 298–314. https://doi.org/10.1130/0016-7606(2002)114<0298:pbeato>2.0.co;2

Leonard, L. J., Currie, C. A., Mazzotti, S., & Hyndman, R. D. (2010). Rupture area and displacement of past Cascadia great earthquakes from coastal coseismic subsidence. *GSA Bulletin*, *122*(11–12), 2079–2096. https://doi.org/10.1130/b30108.1

LeVeque, R. J., George, D. L., & Berger, M. J. (2011). Tsunami modelling with adaptively refined finite volume methods. *Acta Numerica*, *20*, 211–289. https://doi.org/10.1017/s0962492911000043

Li, S., Wang, K., Wang, Y., Jiang, Y., & Dosso, S. E. (2018). Geodetically inferred locking state of the Cascadia megathrust based on a viscoelastic Earth model. *Journal of Geophysical Research: Solid Earth*, *123*(9), 8056–8072. https://doi.org/10.1029/2018jb015620

Lotto, G. C., Dunham, E. M., Jeppson, T. N., & Tobin, H. J. (2017). The effect of compliant prisms on subduction zone earthquakes and tsunamis. *Earth and Planetary Science Letters*, *458*, 213–222. https://doi.org/10.1016/j.epsl.2016.10.050

Lotto, G. C., Jeppson, T. N., & Dunham, E. M. (2019). Fully coupled simulations of megathrust earthquakes and tsunamis in the Japan trench, Nankai Trough, and Cascadia Subduction Zone. *Pure and Applied Geophysics*, *176*(9), 4009–4041. https://doi.org/10.1007/s00024-018-1990-y

Ma, S. (2012). A self-consistent mechanism for slow dynamic deformation and tsunami generation for earthquakes in the shallow subduction zone. *Geophysical Research Letters*, *39*(11), L11310. https://doi.org/10.1029/2012gl051854

Ma, S., & Nie, S. (2019). Dynamic wedge failure and along-arc variations of tsunamigenesis in the Japan trench margin. *Geophysical Research Letters*, *46*(15), 8782–8790. https://doi.org/10.1029/2019gl083148

MacKay, M. E. (1995). Structural variation and landward vergence at the toe of the Oregon accretionary prism. *Tectonics*, *14*(6), 1309–1320. https://doi.org/10.1029/95tc02320

McCrory, P. A., Blair, J. L., Waldhauser, F., & Oppenheimer, D. H. (2012). Juan de Fuca slab geometry and its relation to Wadati-Benioff zone seismicity. *Journal of Geophysical Research*, *117*(B9), B09306. https://doi.org/10.1029/2012jb009407

Melgar, D., Williamson, A. L., & Salazar-Monroy, E. F. (2019). Differences between heterogenous and homogenous slip in regional tsunami hazards modelling. *Geophysical Journal International*, *219*(1), 553–562.

Mori, N., Takahashi, T., Yasuda, T., & Yanagisawa, H. (2011). Survey of 2011 Tohoku earthquake tsunami inundation and run-up. *Geophysical Research Letters*, *38*(7), L00G14. https://doi.org/10.1029/2011gl049210

Peterson, C. D., & Darienzo, M. E. (1996). Discrimination of climatic, oceanic, and tectonic mechanisms of cyclic marsh burial. In Rogers, A. M., Walsh, T. J., Kockelman, W. J., & Priest, G. R. (Eds.), *Assessing earthquake hazards and reducing risk in the Pacific Northwest*. (pp. 115–146).

Peterson, C. D., & Priest, G. R. (1995). Preliminary reconnaissance survey of Cascadia paleotsunami deposits in Yaquina Bay, Oregon. *Oregon Geology*, *57*(2), 33–40.

Priest, G. R., Goldfinger, C., Wang, K., Witter, R. C., Zhang, Y., & Baptista, A. M. (2009). *Tsunami hazard assessment of the Northern Oregon Coast: A multi-deterministic approach tested at Cannon Beach, Clatsop County, Oregon* (Vol. 41, p. 87). Oregon Department of Geology Mineral Industries Special Paper.

Priest, G. R., Myers, E., Baptista, A. M., Fleuck, P., Wang, K., Kamphaus, R. A., & Peterson, C. D. (1997). *Cascadia subduction zone tsunamis: Hazard mapping at Yaquina Bay* (p. 144). Oregon: State of Oregon, Department of Geology and Mineral Industries. Open-File Report O-97-34.

Priest, G. R., Myers, E., Baptista, A. M., Fleuck, P., Wang, K., & Peterson, C. D. (2000). Source simulation for tsunamis: Lessons learned from fault rupture modeling of the Cascadia subduction zone, North America. *Science of Tsunami Hazards*, *18*(2), 77–106.

Ramos, M. D., & Huang, Y. (2019). How the transition region along the Cascadia megathrust influences coseismic behavior: Insights from 2-D dynamic rupture simulations. *Geophysical Research Letters*, *46*(4), 1973–1983. https://doi.org/10.1029/2018gl080812

Ramos, M. D., Huang, Y., Ulrich, T., Li, D., Gabriel, A. A., & Thomas, A. M. (2021). Assessing margin-wide rupture behaviors along the Cascadia megathrust with 3-D dynamic rupture simulations. *Journal of Geophysical Research: Solid Earth*, e2021JB022005. https://doi.org/10.1029/2021jb022005

Royer, A. A., Thomas, A. M., & Bostock, M. G. (2015). Tidal modulation and triggering of low-frequency earthquakes in northern Cascadia. *Journal of Geophysical Research: Solid Earth*, *120*(1), 384–405. https://doi.org/10.1002/2014jb011430

Salaree, A., Huang, Y., Ramos, M. D., & Seth, S. (2021). *Relative tsunami hazard from segments of Cascadia subduction zone for Mw 7.5–9.2 earthquakes*.

Satake, K., Wang, K., & Atwater, B. F. (2003). Fault slip and seismic moment of the 1700 Cascadia earthquake inferred from Japanese tsunami descriptions. *Journal of Geophysical Research*, *108*(B11), 2535. https://doi.org/10.1029/2003jb002521

Schlichting, R. B. (2000). *Establishing the inundation distance and overtopping height of paleotsunami from the late-Holocene geologic record at open-coastal wetland sites, central Cascadia margin*.

Schmalzle, G. M., McCaffrey, R., & Creager, K. C. (2014). Central Cascadia subduction zone creep. *Geochemistry, Geophysics, Geosystems*, *15*(4), 1515–1532. https://doi.org/10.1002/2013gc005172

Shennan, I., Long, A. J., Rutherford, M. M., Green, F. M., Innes, J. B., Lloyd, J. M., et al. (1996). Tidal marsh stratigraphy, sea-level change and large earthquakes, I: A 5000 year record in Washington, USA. *Quaternary Science Reviews*, *15*(10), 1023–1059. https://doi.org/10.1016/s0277-3791(96)00007-8

Tréhu, A. M., Blakely, R. J., & Williams, M. C. (2012). Subducted seamounts and recent earthquakes beneath the central Cascadia forearc. *Geology*, *40*, 103–106. https://doi.org/10.1130/g32460.1

Wang, P. L., Engelhart, S. E., Wang, K., Hawkes, A. D., Horton, B. P., Nelson, A. R., & Witter, R. C. (2013). Heterogeneous rupture in the great Cascadia earthquake of 1700 inferred from coastal subsidence estimates. *Journal of Geophysical Research: Solid Earth*, *118*(5), 2460–2473. https://doi.org/10.1002/jgrb.50101

Wilson, A., & Ma, S. (2021). Wedge plasticity and fully coupled simulations of dynamic rupture and tsunami in the Cascadia subduction zone. *Journal of Geophysical Research: Solid Earth*, *126*(7), e2020JB021627. https://doi.org/10.1029/2020jb021627

Witter, R. C., Zhang, Y. J., Wang, K., Priest, G. R., Goldfinger, C., Stimely, L., et al. (2013). Simulated tsunami inundation for a range of Cascadia megathrust earthquake scenarios at Bandon, Oregon, USA. *Geosphere*, *9*(6), 1783–1803. https://doi.org/10.1130/ges00899.1

Yamaguchi, D. K., Atwater, B. F., Bunker, D. E., Benson, B. E., & Reid, M. S. (1997). Tree-ring dating the 1700 Cascadia earthquake. *Nature*, *389*(6654), 922–923. https://doi.org/10.1038/40048

References From the Supporting Information

Andrews, D. J. (2004). Rupture models with dynamically determined breakdown displacement. *Bulletin of the Seismological Society of America*, *94*(3), 769–775.

Aslam, K. S., & Daub, E. G. (2018). Effect of fault roughness on aftershock distribution: Elastic off-fault material properties. *Journal of Geophysical Research: Solid Earth*, *123*(11), 9689–9711.

Bizzarri, A. (2010). How to promote earthquake ruptures: Different nucleation strategies in a dynamic model with slip-weakening friction. *Bulletin of the Seismological Society of America*, *100*(3), 923–940.

Gao, D., Wang, K., Insua, T. L., Sypus, M., Riedel, M., & Sun, T. (2018). Defining megathrust tsunami source scenarios for northernmost Cascadia. *Natural Hazards*, *94*(1), 445–469.

Harris, R. A., Barall, M., Aagaard, B., Ma, S., Roten, D., Olsen, K., & Ampuero, J. P. (2018). A suite of exercises for verifying dynamic earthquake rupture codes. *Seismological Research Letters*, *89*(3), 1146–1162.

Wech, A. G., & Creager, K. C. (2011). A continuum of stress, strength and slip in the Cascadia subduction zone. *Nature Geoscience*, *4*(9), 624–628.

Van Zelst, I., Wollherr, S., Gabriel, A. A., Madden, E. H., & van Dinther, Y. (2019). Modeling megathrust earthquakes across scales: One-way coupling from geodynamics and seismic cycles to dynamic rupture. *Journal of Geophysical Research: Solid Earth*, *124*(11), 11414–11446.